

Quantum estimation of magnetic-field gradient using W-state

H. T. Ng and K. Kim

*Center for Quantum Information, Institute for Interdisciplinary Information Sciences,
Tsinghua University, Beijing 100084, P. R. China*

(Dated: November 1, 2018)

We study the precision limits of detecting a linear magnetic-field gradient by using W-states in the presence of different types of noises. We consider to use an atomic spin chain for probing the magnetic-field gradient, where a W-state is prepared. We compare this method with the measurement of using two uncorrelated atoms. For pure states, W-states can provide an improvement over uncorrelated states in determining the magnetic-field gradient up to four particles. We examine the effects of local dephasing and dissipations on the performances of detections. In presence of dephasing, the uncorrelated atoms can give a higher precision than using W-states. But W-states provide a better performance in the presence of dissipation for a few particles. We briefly discuss the implementation of the detection methods with cold atoms and trapped ions.

PACS numbers: 03.67.Bg, 03.75.Dg, 07.55.Ge

I. INTRODUCTION

Measurement of magnetic-field gradient is important in magnetic resonance imaging (MRI) [1] and quantum control [2], etc. For example, MRI relies on the principle of nuclear magnetic resonance [3]. The information of an image can be encoded via the magnetic-field gradient [1]. The quality of imaging can be improved by reducing the signal-to-noise ratio of the magnetic-field gradient. Therefore, the methods for the reduction of signal-to-noise ratio may advance the technology of MRI.

Precision measurements of magnetic-field gradient [4–6], which use the different physical systems and entangled states, have recently been proposed. In this paper, we propose to detect the magnetic-field gradient by using an atomic spin chain. Indeed, neutral atoms [7, 8] and trapped ions [9] can be used to accurately determine the frequency standard which are important in science and engineering. Entangled states are useful to enhance the precision of measurements. In addition, the two classes of multipartite entangled states, such as GHZ [10] and W-states [11], have been demonstrated using trapped ions. For example, a W-state has been produced by using a string of 8 trapped ions [11]. More recently, a W-state of a few tens of cold atoms have also been produced in an optical fiber cavity [12].

In realistic situations, the atoms are inevitable to be coupled to the environment. This greatly limits the performance of measurement. For example, GHZ states can only give the same uncertainty of uncorrelated states in detecting the transition frequencies in the presence of dephasing [13]. Recently, the bounds of the measurement errors have been provided [14, 15] in the presence of the different types of noises. In the limit of large number of atoms, the precision limit can be improved by a constant factor in comparison with uncorrelated states irrespective of the initial state and measurement scheme. Therefore, it is important to study the precision limits of the different input states in the presence of the different types of noises.

In this paper, we propose a method to detect the magnetic-field gradient by using a chain of atoms, where the atoms are prepared in a W-state. W-states are genuine multipartite entangled states [16] and are robust against noises and particle losses [11]. We show that the magnetic-field gradient can be encoded onto the coherence of an atomic spin chain. Therefore, it can be used for measuring the magnetic-field gradient. Also, we compare this method with another detection method by using two uncorrelated atoms.

In fact, the precision limits of detecting the magnetic-field gradient by using uncorrelated states and W-states are both inversely proportional to the size of the system. To compare the two methods with the same size, the distance between two separate uncorrelated atoms is equal to the length of a chain of atoms which are prepared in a W-state. We show that W-states can provide an improvement over the method by using uncorrelated states up to four particles.

We investigate the effects of local dephasing and dissipations on these two detection methods. In contrast to the cases of pure states, their performances are different in the presence of the different types of noises. We find that uncorrelated states are able to give better performance than W-states when the dephasing noise is present. However, W-states provide a higher precision than uncorrelated states for a few particles in the presence of dissipation.

This paper is organized as follows: In section 2, we introduce the system of an atomic spin chain and discuss the coupling of atoms to a linear gradient magnetic-field. In section 3, we study the precision limits of using an atomic spin chain for measuring the magnetic-field gradient, where the atoms are in prepared in a W-state. We compare this method with the measurement by using two uncorrelated atoms. In section 4, we investigate the effects of local dephasing and dissipation on the performances of the two different detection methods. In section 5, we briefly discuss the physical realization of a spin chain by using cold atoms and trapped ions. We

provide a summary in section 6. We give out the details of calculations in appendices.

II. DETECTION OF MAGNETIC-FIELD GRADIENT

A. System

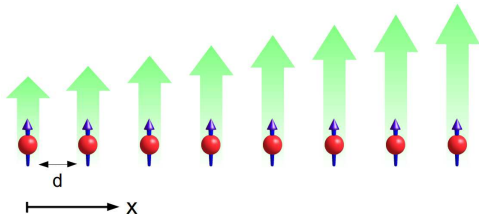


FIG. 1. (Color online) An atomic spin chain is coupled to a linear magnetic-field gradient in the x -direction. Each atom is separated with a distance d .

We consider an atom to have two hyperfine spin states. When an atom is coupled to a magnetic field, the energy splitting between two hyperfine states is changed due to the Zeeman effect [3]. By measuring the difference of the transition frequencies of two atoms at the two different locations, the magnetic-field gradient can be determined. In general, an atomic spin chain can be used for detecting the magnetic-field gradient as shown in Fig. 1, where each atom is equally spaced with a distance d . We assume that the magnetic field $B(x_j)$ linearly varies with the position x_j as

$$B(x_j) = B_1 + Gx_j, \quad (1)$$

where B_1 is the reference magnetic field and G is the magnetic-field gradient. The Hamiltonian, which describes the coupling between atom and the magnetic field, is

$$H = \hbar \sum_{j=1}^N \omega_j \sigma_z^j, \quad (2)$$

where ω_j and σ_z^j are the energy frequency and Pauli operator of atom j . The total number of atoms in the chain is N . The transition frequency ω_j depends on the magnitude of the magnetic field $B(x_j)$ as

$$\omega_j = \omega_0 + \gamma B(x_j), \quad (3)$$

where ω_0 is the transition frequency of the two hyperfine spin states without the external magnetic-field and γ is the gyromagnetic ratio of an atom.

B. Using W-states

We study the detection method by using W-states. Initially, the system is prepared in a W-state which is writ-

ten as

$$\begin{aligned} |W\rangle &= \frac{1}{\sqrt{N}}(|100\dots 0\rangle + |010\dots 0\rangle + \dots + |000\dots 1\rangle), \\ &= \frac{1}{\sqrt{N}} \sum_{j=1}^N |w_j\rangle, \end{aligned} \quad (4)$$

where $|w_j\rangle = |1\rangle_j \prod_{j' \neq j} |0\rangle_{j'}$ and $j' \neq j$. When the atomic chain is coupled to the magnetic-field gradient for a time t , the state becomes

$$|\psi(t)\rangle = \frac{1}{\sqrt{N}} \sum_{j=1}^N e^{-2ij\theta_1 t} |w_j\rangle, \quad (5)$$

where $\theta_1 = G\gamma d$. The global phase factor has been omitted here.

The magnetic-field gradient can be encoded onto the quantum coherence of the state. The quantum coherence factor C_1 can be defined as

$$C_1 = N|W\rangle\langle W| - \sum_{j=1}^N |w_j\rangle\langle w_j|. \quad (6)$$

Now $\langle C_1 \rangle$ can be expressed as:

$$\langle C_1 \rangle = -1 + \frac{1}{N} \frac{\sin^2(N\theta_1 t)}{\sin^2(\theta_1 t)}. \quad (7)$$

The quantity $\langle C_1 \rangle$ is a function of the parameter θ_1 which is proportional to the gradient G . Therefore, the magnetic-field gradient can be determined from the coherence $\langle C_1 \rangle$. The details of the derivation of Eq. (7) is provided in Appendix A. In fact, the quantity $\langle C_1 \rangle$ can be obtained by averaging the terms $\langle \prod_{k \neq i, j} |0\rangle_{kk} \langle 0| \langle \sigma_-^i \sigma_+^j + \sigma_-^j \sigma_+^i \rangle$ which can be experimentally measured.

In Fig. 2, we plot the coherence $\langle C_1 \rangle$ versus time, for the different number of atoms N . The small oscillations are observed when $\langle C_1 \rangle$ is about -1. The peaks occur when the dimensionless time $\theta_1 t$ is a multiple of π . The maximum of peaks can attain $N - 1$.

The magnetic-field gradient can be determined from the coherence $\langle C_1 \rangle$. The uncertainty $\delta\Theta_1$ of the measurement is

$$\begin{aligned} \delta\Theta_1 &= \frac{\Delta C_1}{\left| \frac{\partial \langle C_1 \rangle}{\partial \Theta_1} \right|}, \quad (8) \\ &= \frac{[N^2 \sin^2 \Theta_1 - \sin^2(N\Theta_1)]^{1/2} |\sin(N\Theta_1)|}{|N \sin(2N\Theta_1) - 2 \cot \Theta_1 \sin^2(N\Theta_1)|}. \quad (9) \end{aligned}$$

where $\Theta_1 = \theta_1 t$ and $\Delta C_1 = \sqrt{\langle C_1^2 \rangle - \langle C_1 \rangle^2}$.

The minimum of uncertainty $\delta\Theta_{\min}$ is obtained

$$\delta\Theta_1^{\min} = \frac{1}{2} \sqrt{\frac{3}{N^2 - 1}}, \quad (10)$$

when $\Theta_1 = n\pi$ and n is an integer. The minimum uncertainty is proportional to N^{-1} for large N . The minimum uncertainty in Eq. (10) can be intuitively understood from the time-energy uncertainty relation [17]. The

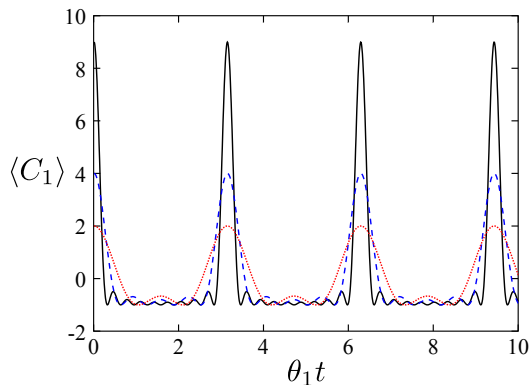


FIG. 2. (Color online) $\langle C_1 \rangle$ versus time $\theta_1 t$, for the different number of atoms N . The different number of atoms N are denoted by the different lines: $N = 3$ (red-dotted), $N = 5$ (blue-dashed) and $N = 10$ (red-solid), respectively.

minimum uncertainty $\delta\Theta_{\min}$ occurs when the energy fluctuation of the state is maximum. The bound in Eq. (10) can be derived from the time-energy uncertainty which is given in Appendix B.

C. Using two uncorrelated atoms

We study the measurement of magnetic-field gradient by using two uncorrelated atoms which are separated with a distance D as shown in Fig. 3. We will compare the precision limits of using two uncorrelated atoms and an atomic chain with the same system's size D . To facilitate our subsequent discussion, we set $D = (N - 1)d$, where N is the number of atoms in the chain.

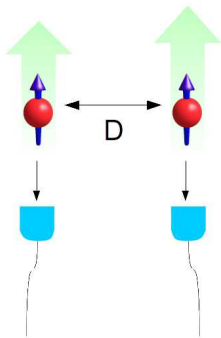


FIG. 3. (Color online) Two uncorrelated atoms are separate with a distance D for measuring the magnetic-field gradient. The two different magnetic fields are independently measured.

The magnetic-field gradient can be determined by individually measuring two atoms at the two different positions. The magnetic-field gradient is

$$G = \frac{B_2 - B_1}{D}, \quad (11)$$

where B_2 and B_1 are the magnetic fields at the two different positions.

Now, we briefly describe the procedures of measurement. Initially, the atoms are prepared in the equally weighted superpositions as

$$|\Psi(0)\rangle_j = \frac{1}{\sqrt{2}}(|0\rangle_j + |1\rangle_j), \quad (12)$$

where $j = 1$ and 2 . Then, let the system freely evolve for a time t . The state becomes

$$|\Psi(t)\rangle_j = \frac{1}{\sqrt{2}}(e^{i\omega_j t}|0\rangle_j + e^{-i\omega_j t}|1\rangle_j). \quad (13)$$

By applying a $\pi/2$ -pulse to the atom, the state can be written as

$$|\Psi'(t)\rangle_j = \frac{1}{2}e^{i\omega_j t}[(1 - e^{2i\omega_j t})|0\rangle + (1 + e^{-2i\omega_j t})|1\rangle]. \quad (14)$$

The frequency ω_j can be determined by measuring the probability P_j of the state $|1\rangle_j$ which is given by

$$P_j = \frac{1}{2}(1 + \cos 2\omega_j t). \quad (15)$$

The uncertainty $\delta\omega_j$ is given by [13]

$$\delta\omega_j = \sqrt{P_j(1 - P_j)} \left| \frac{dP}{d\omega_j} \right|^{-1}, \quad (16)$$

$$= \frac{1}{2t} \left[\frac{1 - \cos^2(2\omega_j t)}{\sin^2(2\omega_j t)} \right]^{1/2}. \quad (17)$$

When $t = m\pi/\omega'_j$, the minimum uncertainty can be obtained, where m is an odd integer. The minimum uncertainty $\delta\omega_j^{\min}$ is

$$\delta\omega_j^{\min} = \frac{1}{2t}. \quad (18)$$

The uncertainty of the gradient is proportional to the sum of $\delta\omega_1$ and $\delta\omega_2$,

$$\delta G = \frac{\sqrt{\delta\omega_2^2 + \delta\omega_1^2}}{\gamma D}, \quad (19)$$

where $\delta\omega_j = \gamma\delta B_j$. We can express the uncertainty $\delta\theta_2$ as

$$\delta\theta_2 = \frac{\sqrt{\delta\omega_2^2 + \delta\omega_1^2}}{N - 1}, \quad (20)$$

where $\theta_2 = \gamma G d$ and $D = (N - 1)d$. From Eqs. (18) and (20), the minimum uncertainty $\delta\Theta_2^{\min}$ is

$$\delta\Theta_2^{\min} = \frac{1}{\sqrt{2}(N - 1)}, \quad (21)$$

where $\Theta_2 = \theta_2 t$.

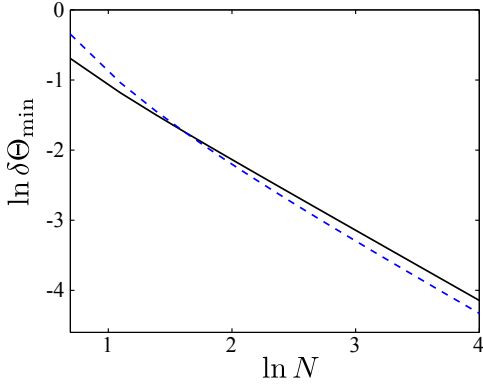


FIG. 4. (Color online) Log-log plot of $\delta\Theta_{\min}$ versus N . The W-states and uncorrelated states are denoted with black solid and blue dashed lines, respectively.

D. Comparison of two methods

Now we compare the performances of these two methods. In Fig. 4, we plot the minimum uncertainties of uncorrelated states with the two different methods. Although the uncertainties of the two methods both scale with N^{-1} if N is large. W-states can provide a higher precision than using uncorrelated atoms up to 4 particles.

In addition, it should be noted that the improving factor N^{-1} comes from the gradient field which gives rise to the energy fluctuation of the state of order of N . The uncorrelated states can also provide the scaling N^{-1} . Therefore, in this sense, the scaling of N^{-1} is different to the usual Heisenberg-limited measurement [18].

III. EFFECTS OF DEPHASING AND DISSIPATION

Now we study the effects of local dephasing and dissipation of atoms on measurements. We consider each atom to be independently coupled to the bath. We have assumed that the Markovian approximation is valid. The master equation of atom j , which describes dissipation and dephasing at low temperature, is written as [19]

$$\begin{aligned} \dot{\rho}^{(j)} = & i[\rho^{(j)}, H] + \Gamma_p(\sigma_z^j \rho^{(j)} \sigma_z^j - \rho) + \frac{\Gamma_d}{2}(2\sigma_-^j \rho^{(j)} \sigma_+^j \\ & - \sigma_+^j \sigma_-^j \rho^{(j)} - \rho^{(j)} \sigma_+^j \sigma_-^j), \end{aligned} \quad (22)$$

where Γ_p and Γ_d are the dephasing and dissipation rates, respectively. The dissipative dynamics can be solved as: $\rho_{11}^{(j)} = e^{-\Gamma_d t} \rho_{11}^{(j)}(0)$, $\rho_{00}^{(j)} = 1 - e^{-\Gamma_d t} \rho_{11}^{(j)}(0)$ and $\rho_{01}^{(j)} = e^{-\frac{\Gamma_d}{2} t - \Gamma_p t + 2i\omega_j t} \rho_{01}^{(j)}(0)$.

The system becomes incoherent and the dynamics is no longer periodic. Therefore, the precision limits are limited due to noises. For W-states, we can obtain the analytical expression of the uncertainty of the parameter θ_1 in the presence of dissipation and dephasing, It is given

by

$$\delta\theta_1 = \frac{[g_1(t) \sin^4 \Theta_1 + g_2(t) \sin^2 \Theta_1 \sin^2(N\Theta_1) - \sin^4(N\Theta_1)]^{\frac{1}{2}}}{t|N \sin(2N\Theta_1) - 2 \cot \Theta_1 \sin^2(N\Theta_1)|}, \quad (23)$$

where $g_1(t) = N^2[(N-1)e^{(2\Gamma-\Gamma_d)t} - (N-2)e^{\Gamma t} - 1]$, $g_2(t) = [N(N-2) + 2Ne^{-\Gamma t}]e^{\Gamma t}$ and $\Gamma = \Gamma_d + 2\Gamma_p$.

For uncorrelated atoms, the uncertainty is given by

$$\delta\theta_2 = \frac{1}{t(N-1)} \left[\sum_{j=1}^2 \frac{1 - e^{-\Gamma t} \cos^2(2\omega_j t)}{4e^{-\Gamma t} \sin^2(2\omega_j t)} \right]^{1/2}, \quad (24)$$

where $\Gamma = \Gamma_d + 2\Gamma_p$. From Eq. (24), the minimum uncertainty occurs when $t = \Gamma^{-1}$ and $\omega_j t = n\pi/2$, where n is odd. It is given by

$$\delta\theta_2^{\min} = \frac{1}{N-1} \sqrt{\frac{\Gamma^2 e}{2}}. \quad (25)$$

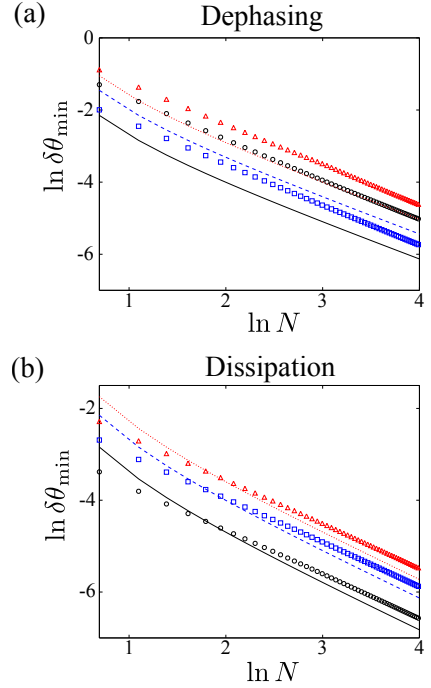


FIG. 5. (Color online) Log-log plot of $\delta\theta_{\min}$ versus N . The dimensionless time θt is used. The cases of dephasing and dissipation are shown in (a) and (b), respectively. The different dephasing (Γ_p) and dissipation (Γ_d) rates, using W-states, are denoted by the different symbols: 0.05θ (black circle), 0.10 (blue square) and 0.15θ (red triangle), respectively. The measurements, using uncorrelated atoms, are denoted by the different lines: 0.05θ (black solid), 0.10 (blue dashed) and 0.15θ (red dotted), respectively.

We numerically search the local minimum of the uncertainties in Eq. (23) within the dimensionless time interval, $\theta\Delta t$, between 0 and π , where the smallest time step is up to 10^{-7} . There exists a minimum point around $\theta_1 t = \pi$ but the time interval is shorter than 10^{-7} . We have abandoned those points which are unstable (the first

derivative of those points vary rapidly instead of being zeros).

We compare the performance of using uncorrelated states and W-states in Fig. 5. We plot $\delta\theta_{\min}$ versus N on a logarithmic scale, for the different dephasing and dissipation rates in Figs. 5 (a) and (b), respectively. If the dephasing and dissipation rates are much smaller than the parameter of magnetic-field gradient, than $\ln\delta\phi_{\min}$ of W-states is proportional to $\ln N$ and the slope is about -1. The uncertainty is proportional to N^{-1} .

For pure states, W-states can provide a higher precision than uncorrelated states up to 4 particles. In Fig. 5(a), the uncorrelated states can do better than W-states in the presence of dephasing. In Fig. 5(b), the precision limits of W-states and uncorrelated states in the presence of dissipations are plotted. W-states can provide a higher precision than uncorrelated states for a few particles. This result shows that the different precision limits of W-states and uncorrelated states can be obtained in the presence of the different types of noises.

IV. DISCUSSION

Let us briefly discuss the methods of realizations of a spin chain using cold atoms and trapped ions, respectively. An atomic spin chain can be realized by using ultracold atoms in an optical lattice [23]. Indeed, an atomic spin chain has recently been shown by using a bosonic Mott insulator. In principle, an order of hundred of atoms can be confined in a 1D lattice. However, this may be difficult to load exactly one atom into every lattice site. To produce a W-state in an optical lattice, nonlocal interactions between the atoms are necessary. This can be made by coupling the atoms to a cavity mode [12]. In fact, the atoms, strongly coupling to a cavity mode, have been demonstrated in experiments [12, 24, 25]. Also, the W-states can be generated in a spin chain with ferromagnetic interaction [26]. The specific spin-spin interactions can be engineered in optical lattices.

Alternatively, a spin chain can be implemented by using trapped ions. In fact, a W-state has been created in a string of trapped ions [11] which can be used for detecting the magnetic-field gradient. An order of several tens of ions [27] can be realized in the near future. However, the distance between ions are not equally spaced. Also, micromotions of ions may introduce an additional noise to the measurements. This may be resolved by either using an anharmonic linear trap [28] or combining an additional optical lattice [29] to adjust the position of ions.

Next, we discuss the measurements of estimators by using the two different methods. In the uncorrelated case, it is necessary to perform two independent measurements at the two ends for the gradient-field measurement. By using a W-state, the magnetic-field gradient can be determined by just measuring the coherence factor. To fa-

cilitate our discussion, we write a collection of qubits in terms of angular momentum operators (J_x, J_y, J_z) . It is easy to show that the coherence factor C_1 can be related to J_x^2 plus a constant, where $J_x = \sum_i \sigma_x^i$. To probe the variance J_x^2 , all qubits can be coupled to a polarized light. The correlation information can be mapped onto the output field. Thus, the variance J_x^2 can be determined by a collective quantum-nondemolition measurement. This detection method has been proposed [30]. In this way, the effort of measurement on the qubits can be much reduced. Bearing in mind that the generation of W-states in a cavity can benefit from collective measurements in [12]. This method may offer the advantages by using advanced experimental techniques in quantum optics such as collective quantum-nondemolition measurements [30] and cavity enhanced interactions [12].

In addition, this scheme can be generalized to detect the nonlinear gradient field. For example, the magnetic field $B(x)$ is proportional to x^α , where x is the position and α is the power. The uncertainty of magnetic-field gradient is proportional to $1/N^\alpha$. It is because the uncertainty of the parameter is proportional to the energy fluctuation of the gradient field. This is similar to the discussion for a linear field in the Appendix.

V. CONCLUSION

In summary, we have studied and compared the two different methods on measurement of magnetic-field gradient by using cold atoms. We investigate an atomic chain, which is prepared in a W-state, for detection the magnetic-field gradient. We also study the detection method by using two uncorrelated atoms. For pure states, W-states can provide a higher precision than uncorrelated states. In addition, we have studied the effect of local dephasing and dissipations on the performances of the two different detection methods. In contrast to the cases of pure states, we find that uncorrelated atoms can provide a better performance than using W-states in the presence of dephasing. But W-states can provide a higher precision than uncorrelated states for a few particles if the dissipation is present. This result shows that the precision limits are greatly changed due to the different types of noises. Finally, we have briefly discussed the methods of realizations using cold atoms and trapped ions.

ACKNOWLEDGMENTS

We thank for Iñigo Urizar-Lanz, Iagoba Apellaniz, and Geza Toth for their useful comments. This work was

supported in part by the National Basic Research Program of China Grant 2011CBA00300, 2011CBA00301, 2011CBA00302 the National Natural Science Founda-

tion of China Grant 11304178, 61073174, 61033001, 61061130540, 61361136003. KK acknowledges the support from young 1000 plan.

-
- [1] P. C. Lauterbur, *Nature* **242**, 190 (1973).
 [2] M. S. Grinolds *et al.* *Nat. Phys.* **7**, 687 (2011).
 [3] P. Glover and P. Mansfield, *Rep. Prog. Phys.* **65**, 1489 (2002).
 [4] H. T. Ng, *Phys. Rev. A* **87**, 043602 (2013).
 [5] I. Urizar-Lanz *et al.*, *Phys. Rev. A* **88**, 013626 (2013).
 [6] F. Schmidt-Kaler, R. Gerritsma, *Europhys. Lett.* **99**, 53001 (2012).
 [7] N. Hinkley *et al.*, *Science* **341**, 1215 (2013).
 [8] B. J. Bloom *et al.*, *Nature* **506**, 71 (2014).
 [9] T. Rosenband *et al.*, *Science* **319**, 1808 (2008).
 [10] T. Monz *et al.*, *Phys. Rev. Lett.* **106**, 130506 (2011).
 [11] H. Häffner *et al.*, *Nature* **438**, 643 (2005).
 [12] F. Haas, J. Volz, R. Gehr, J. Reichel, J. Estève, *Nature* **344**, 80 (2014).
 [13] S. F. Huelga *et al.*, *Phys. Rev. Lett.* **79** 3865 (1997).
 [14] B. M. Escher, R. L. de Matos Filho and L. Davidovich, *Nat. Phys.* **7**, 406 (2011).
 [15] R. Demkowicz-Dobrzański, J. Kolodyński and M. Gutů, *Nat. Commun.* **3**, 1063 (2012).
 [16] W. Dür, G. Vidal and J. I. Cirac, *Phys. Rev. A* **62**, 062314 (2000).
 [17] V. Giovannetti, S. Lloyd, L. Maccone, *Phys. Rev. Lett.* **96**, 010401 (2006).
 [18] V. Giovannetti, S. Lloyd, L. Maccone, *Science* **306**, 1330 (2004).
 [19] S. M. Barnett and P. M. Radmore, *Methods in Theoretical Quantum Optics* (Oxford University Press, Oxford, 2002).
 [20] I. Bloch, J. Dalibard, W. Zwerger, *Rev. Mod. Phys.* **80** 885 (2008).
 [21] J. Simon *et al.* *Nature* **472**, 307 (2011).
 [22] M. Endres *et al.*, *Science* **334**, 200 (2011).
 [23] T. Fukuhara *et al.*, *Nat. Phys.* **9** 235 (2013).
 [24] F. Brennecke, T. Donner, S. Ritter, T. Bourdel, M. Köhl, T. Esslinger, *Nature* **450** 268 (2007).
 [25] Y. Colombe, T. Steinmetz, G. Dubois, F. Linke, D. Hunger and J. Reichel, *Nature* **450**, 272 (2007).
 [26] D. Bruß, N. Datta, A. Ekert, L. C. Kwek, and C. Macchiavello, *Phys. Rev. A* **72**, 014301 (2005).
 [27] R. Islam *et al.*, *Science* **340**, 583 (2013).
 [28] G.-D. Lin *et al.* *Europhys. Lett.* **86** 60004 (2009).
 [29] R. B. Linnet, I. D. Leroux, M. Marcianti, A. Dantan, and M. Drewsen, *Phys. Rev. Lett.* **109**, 233005 (2012).
 [30] K. Eckert, O. Romero-Isart, M. Rodriguez, M. Lewenstein, E. S. Polzik, A. Sanpera, *Nat. Phys.* **4**, 50 (2008).
 [31] The formula can be found from the webpage: <http://functions.wolfram.com/01.06.23.0005.01>

Appendix A: Derivation of expectation value and variance of the coherence

We provide a closed form for the summation of cosine functions [31]. We write

$$\sum_{j'=1}^{N-1} \sum_{j=j'+1}^N \cos[2(j'-j)\theta_1 t] = \sum_{j'=1}^{N-1} \sum_{j=1}^{j'} \cos(2j\theta_1 t) \quad (\text{A1})$$

From the Dirichlet kernel, we have

$$1 + 2 \sum_{j=1}^{j'} \cos(2j\theta_1 t) = \frac{\sin[(2j'+1)\theta_1 t]}{\sin(\theta_1 t)}, \quad (\text{A2})$$

$$\sum_{j=1}^{j'} \cos(2j\theta_1 t) = \frac{1}{2} \left[\frac{\sin[(2j'+1)\theta_1 t]}{\sin(\theta_1 t)} - 1 \right]. \quad (\text{A3})$$

Thus,

$$\begin{aligned} & \sum_{j'=1}^{N-1} \sum_{j=1}^{j'} \cos(2j\theta_1 t) \\ &= -\frac{N-1}{2} + \frac{1}{2 \sin(\theta_1 t)} \sum_{j'=1}^{N-1} \sin[(2j'+1)\theta_1 t]. \end{aligned} \quad (\text{A4})$$

Also, from the identity,

$$\sum_{j'=1}^N \sin[(2j'-1)\theta_1 t] = \csc(\theta_1 t) \sin^2(N\theta_1 t), \quad (\text{A5})$$

and therefore

$$\begin{aligned} & \sum_{j'=1}^{N-1} \sin[(2j'+1)\theta_1 t] \\ &= \sum_{j'=1}^N \sin[(2j'-1)\theta_1 t] - \sin(\theta_1 t), \end{aligned} \quad (\text{A6})$$

$$= \csc(\theta_1 t) \sin^2(N\theta_1 t) - \sin(\theta_1 t). \quad (\text{A7})$$

Substitute Eq. (A7) into Eq. (A4), we obtain

$$\sum_{j'=1}^{N-1} \sum_{j=1}^{j'} \cos(2j\theta_1 t) = -\frac{N}{2} + \frac{\sin^2(N\theta_1 t)}{2 \sin^2(\theta_1 t)}. \quad (\text{A8})$$

From Eq. (A8), $\langle C_1 \rangle$ is given by

$$\langle C_1 \rangle = \frac{2}{N} \sum_{j=1}^{N-1} \sum_{j'=j+1}^N \cos[2(j'-j)\theta_1 t], \quad (\text{A9})$$

$$= -1 + \frac{1}{N} \frac{\sin^2(N\theta_1 t)}{\sin^2(\theta_1 t)}, \quad (\text{A10})$$

and $\langle C_1^2 \rangle$ is

$$\begin{aligned} & \langle C_1^2 \rangle \\ &= N - 1 + \frac{2(N-2)}{N} \sum_{j'=1}^{N-1} \sum_{j=1}^{j'} \cos(2j\theta_1 t), \quad (\text{A11}) \end{aligned}$$

$$= N - 1 + \frac{2(N-2)}{N} \left[-\frac{N}{2} + \frac{\sin^2(N\theta_1 t)}{2\sin^2(\theta_1 t)} \right], \quad (\text{A12})$$

$$= 1 + \frac{(N-2)\sin^2(N\theta_1 t)}{N\sin^2(\theta_1 t)}. \quad (\text{A13})$$

The derivative of $\langle C_1 \rangle$, with respect to θ_1 , is

$$\begin{aligned} & \frac{\partial}{\partial \theta_1} \langle C_1 \rangle \\ &= \frac{t}{N\sin^2(\theta_1 t)} [N\sin 2N\theta_1 t - 2\cot(\theta_1 t)\sin^2(N\theta_1 t)]. \quad (\text{A14}) \end{aligned}$$

Appendix B: Bound of uncertainty from time-energy uncertainty relation

We can obtain the bound of uncertainty $\delta\Theta$ from the time-energy uncertainty relation [17]:

$$\delta\varphi\delta E \leq \frac{1}{2\sqrt{M}}, \quad (\text{B1})$$

where $\delta\varphi$ and δE are the uncertainties of the time φ and energy of the input state, respectively, and M is the number of times for repeating the experiments.

We calculate the variance of the energy Hamiltonian in Eq. (2). The expectation values $\langle H \rangle$ and $\langle H^2 \rangle$ are given by

$$\langle H \rangle = \langle W|H|W \rangle, \quad (\text{B2})$$

$$= \frac{\hbar}{N}(2-N) \sum_j \omega_j, \quad (\text{B3})$$

$$\langle H^2 \rangle = \langle W|H^2|W \rangle, \quad (\text{B4})$$

$$\frac{\hbar^2}{N} \left[4 \sum_j \omega_j^2 + (N-4) \left(\sum_j \omega_j \right)^2 \right], \quad (\text{B5})$$

where $\omega_j = \omega_0 + \gamma(j-1)d$. The summations of ω_j and ω_j^2 are

$$\sum_j \omega_j = \omega_0 N + \frac{\gamma d}{2} N(N-1), \quad (\text{B6})$$

$$\begin{aligned} \sum_j \omega_j^2 &= \omega_0^2 N + \gamma d \omega_0 N(N-1) \\ &+ (\gamma d)^2 \left[\frac{1}{6} N(N+1)(2N-5) + N \right]. \quad (\text{B7}) \end{aligned}$$

By using Eqs (B3)-(B7), the variance $\delta E = \Delta H$ is given by

$$\Delta H = (\hbar\gamma d) \sqrt{\frac{N^2-1}{3}}. \quad (\text{B8})$$

From Eq. (B8), we can obtain the bound of $\delta\Theta = \gamma d \delta\varphi / \hbar$ as

$$\delta\Theta_{\min} = \frac{\hbar}{2\Delta H}, \quad (\text{B9})$$

$$= \frac{1}{2} \sqrt{\frac{3}{N^2-1}}. \quad (\text{B10})$$

We find that this expression in Eq. (B10) coincides the bound in Eq. (10). This means that the estimator C_1 in Eq. (6) can give out the best precision.

Appendix C: Expectation values and variances in the presence of dephasing and dissipation

The expression of $\langle C_1 \rangle$, $\langle C_1^2 \rangle$ and $\frac{\partial}{\partial \theta_1} \langle C_1 \rangle$, in the presence of dephasing and dissipation, are given by

$$\begin{aligned} & \langle C_1 \rangle \\ &= \frac{2}{N} \sum_{j=1}^{N-1} \sum_{j'=j+1}^N \cos[2(j'-j)\theta_1 t] e^{-\Gamma t}, \quad (\text{C1}) \end{aligned}$$

$$= \left[-1 + \frac{1}{N} \frac{\sin^2(N\theta_1 t)}{\sin^2(\theta_1 t)} \right] e^{-\Gamma t}. \quad (\text{C2})$$

$$\begin{aligned} & \langle C_1^2 \rangle \\ &= \frac{2(N-2)}{N} \sum_{j=1}^{N-1} \sum_{j'=j+1}^N \cos[2(j'-j)\theta_1 t] e^{-\Gamma t} \\ &+ (N-1)e^{-\Gamma at}, \quad (\text{C3}) \end{aligned}$$

$$= (N-1)e^{-\Gamma at} + \left[1 + \frac{N-2}{N} \frac{\sin^2(N\theta_1 t)}{\sin^2(\theta_1 t)} \right] e^{-\Gamma t}, \quad (\text{C4})$$

$$\begin{aligned} & \frac{\partial}{\partial \theta_1} \langle C_1 \rangle \\ &= \frac{te^{-\Gamma t}}{N\sin^2(\theta_1 t)} [N\sin(2N\theta_1 t) - 2\cot(\theta_1 t)\sin^2(N\theta_1 t)], \quad (\text{C5}) \end{aligned}$$

where $\Gamma = \Gamma_d + 2\Gamma_p$.